

Nonvolatile Electric Field Control of Thermal Magnons in the Absence of an Applied Magnetic Field

Eric Parsonnet¹, Lucas Caretta,² Vikram Nagarajan,¹ Hongrui Zhang,² Hossein Taghinejad,¹ Piush Behera,^{2,4} Xiaoxi Huang,² Pravin Kavle,² Abel Fernandez,² Dmitri Nikonov,³ Hai Li,³ Ian Young,³ James Analytis,¹ and Ramamoorthy Ramesh^{1,2,4}

¹*Department of Physics, University of California, Berkeley, California 94720, USA*

²*Department of Materials Science and Engineering, University of California, Berkeley, California 94720, USA*

³*Components Research, Intel Corporation, Hillsboro, Oregon 97124, USA*

⁴*Material Science Division, Lawrence Berkeley National Laboratory, Berkeley, California 94720, USA*

 (Received 7 January 2022; revised 7 March 2022; accepted 27 May 2022; published 15 August 2022)

Spin transport through magnetic insulators has been demonstrated in a variety of materials and is an emerging pathway for next-generation spin-based computing. To modulate spin transport in these systems, one typically applies a sufficiently strong magnetic field to allow for deterministic control of magnetic order. Here, we make use of the well-known multiferroic magnetoelectric, BiFeO₃, to demonstrate nonvolatile, hysteretic, electric-field control of thermally excited magnon current in the absence of an applied magnetic field. These findings are an important step toward magnon-based devices, where electric-field-only control is highly desirable.

DOI: [10.1103/PhysRevLett.129.087601](https://doi.org/10.1103/PhysRevLett.129.087601)

In the field of magnonics, spin waves, rather than electrons, form the fundamental operating unit [1–4]. The field has experienced rapid growth over the last decade as exciting progress has yielded a breadth of interesting physics as well as the potential for low power dissipation in computing [5]. In lieu of an electronic current, insulating magnetic materials can host magnon currents, which carry spin information and avoid Ohmic losses associated with electron transport. Such materials are well suited for wave-based computing based on magnon logic [6–10]. Indeed, theoretical work has proposed antiferromagnetic spin wave field-effect transistors [11] and realizations of all-magnon transistors based on magnon-magnon scattering with resonant excitation have already been experimentally demonstrated [9]. There are several ways to create magnons [1,4,12–14], and spin transport via magnon currents have already been reported in a variety of magnetic systems [5,15–19]. Though resonant excitations are typically used to study spin waves [20,21], magnon currents can be excited incoherently by a thermal gradient through the spin Seebeck effect (SSE) [22]. While other near-dc-frequency incoherent excitation mechanisms exist [12,23], thermal excitation of magnons is better suited to materials with complex domain structure since it does not require long-range magnetic order [24]. Previous research has demonstrated nonlocal spin transport [25] in insulating ferrimagnets [12,26,27] and antiferromagnets [5,15,18,19,28,29], thermally excited spin transport over exceptionally long distances [30,31], and non-volatile magnetic field control [19]. Electric field control of magnon spin transport, however, has

been limited to concurrent application of high magnetic fields [24]. For operational devices based on magnon transport, electric field control in the absence of an applied magnetic field could be a crucial advance for the field.

Here, we make use of the well-known multiferroic material, BiFeO₃ (BFO), to demonstrate such electric field control of thermal magnons. BFO is a room-temperature magnetoelectric with a large ferroelectric polarization ($\sim 90 \mu\text{C}/\text{cm}^2$), *G*-type antiferromagnetic ordering, and a weak ferromagnetic moment arising from the Dzyaloshinskii-Moriya interaction [32–34]. The ferroelectric and antiferromagnetic domain structures in BFO exhibit a one-to-one correspondence [35], and deterministic control of magnetic order via manipulation of the ferroelectric state (with applied electric fields) has already been demonstrated [36–38], making BFO an attractive option for high-speed, low energy computing [39–42]. Previous work on BFO [43,44] has revealed broad tunability of the magnon dispersion with applied electric field, and early theoretical work predicted all electrical switching of magnon propagation [45].

In this Letter, we demonstrate a novel manifestation of magnetoelectric coupling in BFO to manipulate magnon current. Magnons are excited via the SSE and detected via the inverse spin Hall effect (ISHE) [46,47]. We demonstrate nonvolatile, hysteretic, bistable states of magnon current and establish a robust means of switching between the two states with an applied electric field. Via piezoresponse force microscopy (PFM), we reveal the switching pathway of the ferroelectric order, which is accompanied by the switching

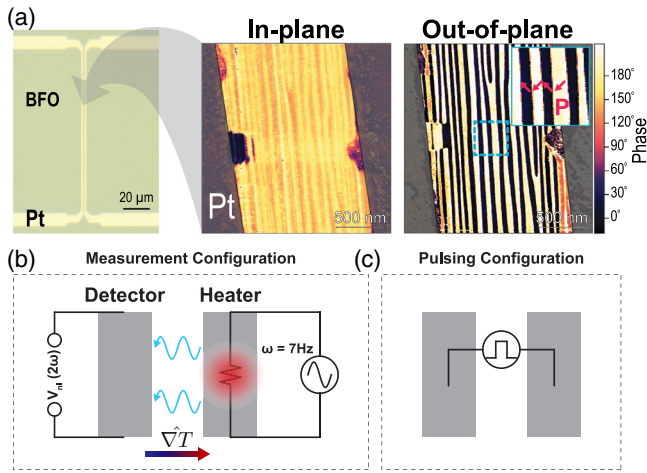


FIG. 1. Experimental setup. (a) Optical and PFM images of nonlocal device structure. Out-of-plane and in-plane PFM images reveal a well-ordered 109° domain structure. Arrows in inset (OOP) show IP projection of spontaneous polarization, \mathbf{P} . (b) Measurement configuration. (c) Pulsing configuration.

of net canted magnetic moment, providing the mechanism for electric field control of magnon current.

We grow BFO samples via pulsed laser deposition (Supplemental Material [48], methods) and employ a nonlocal device geometry [Fig. 1(a)] consisting of two lithographically defined (Supplemental Material [48], methods) Pt wires separated by a distance $d (\leq 1 \mu\text{m})$ on the BFO surface. In the channel between the Pt electrodes, we observe well-ordered 109° ferroelectric domains [Fig. 1(a)]. This confirms the high quality of the BFO film and, via the established correspondence between ferroelectric and magnetic order, allows us access to the magnetic domain structure of the device [35,38,49]. Each of the four leads [Fig. 1(a)] is wire bonded for the nonlocal measurement, described next. In the “measurement configuration,” low-frequency ac current, $f = 7 \text{ Hz}$, driven through the injector Pt wire [Fig. 1(b)] creates a thermal gradient in the film via Joule heating of the Pt (heater) wire. This thermal gradient excites magnons via the SSE. The resulting magnon current is detected at the detector Pt wire as a voltage along the length of the wire, originating from ISHE and spin scattering at the Pt/BFO interface [12,47,50]. We use the standard lock-in technique to measure the magnon current as a differential voltage along the detector wire, V_{nl} . Since the thermal magnon current scales with the square of the charge current in the injector wire, we measure the second harmonic of the detected voltage, i.e., $V_{nl}(2\omega)$ (Supplemental Material [48], methods, which includes reference to data acquisition software [51]).

We confirm the efficacy of our device structure and nonlocal [measurement configuration, Fig. 1(a)] testing protocol by fabricating identical devices on $\text{Y}_3\text{Fe}_5\text{O}_{12}$ (YIG) (Supplemental Material [48]) and performing the prototypical in-plane magnetic-field dependent nonlocal measurement (Supplemental Material [48], Fig. S1), which

shows the expected behavior [12]. To modulate the magnon current in BFO in the absence of an applied magnetic field, we perform *in-situ* electric-field pulsing across the channel [“pulsing configuration,” Fig. 1(a)] thereby switching the ferroelectric, and, consequently, magnetic order parameters (see Supplemental Material [48], for an explanation of magnetic field dependent measurements in BFO, which includes Ref. [52]).

We follow an experimental protocol [Fig. 2(b)] designed to both confirm the switching of the ferroelectricity and monitor resulting changes in the detected magnon current. Following a unipolar (5 ms, 350 kV/cm) voltage pulse in the pulsing configuration, we measure the second harmonic voltage on the detector wire, $V_{nl}(2\omega)$, in the measurement configuration. We then confirm the ferroelectric state by measuring a single bipolar ferroelectric hysteresis (PE) loop. As observed [Fig. 2(b)], the PE loop shows only one switching event (e.g., only showing switching in the positive direction, following negative poling) confirming that the ferroelectric state is both switched and remnant. We then switch the pulse polarity and start again. By alternating positive and negative polarity electric field pulses [Fig. 2(c)] one can clearly observe two nonvolatile states of measured magnon current.

Owing to the ISHE detection mechanism, the Pt detector wire acts as a directional detector, sensitive to the component of incident magnon spin polarization orthogonal to the length of the wire [Fig. 2(a)] [5,12,19]. The existence of two states of magnon current, therefore, indicates that the electric field induced switching results in changes to the magnon spin polarization pointing across the channel. Our results thus indicate that the switching of the ferroelectricity induces switching of the net canted moment (\mathbf{M}) adjacent to the detector Pt wire. As a result, the spin polarization of thermally excited magnons along \mathbf{M} , also flips, resulting in the observed change in detected nonlocal voltage. To better understand the mechanism of such switching, we turn to PFM to directly image the ferroic order.

It has been shown previously [53], that there is one-to-one correspondence between ferroelectric domains and antiferromagnetic domains in BFO, so, via PFM we are able to intuit the magnetic domain structure. Within a single domain, the ferroelectric polarization, Néel vector, and canted ferromagnetic moment are oriented orthogonal to one another [Fig. 3(a)] with the in-plane projection of the canted moment pointing along the in-plane projection of the ferroelectric polarization [36,54,55]. Owing to mechanical and electrostatic boundary conditions [49], adjacent domains’ polarization vectors are oriented 109° from each other and aligned head to tail [Fig. 3(a)]. The existence of such 109° domains is confirmed via PFM in our films [Fig. 1(a)], and results in a net canted moment (along $\langle 100 \rangle_{pc}$), which points orthogonal to the directionality ($\langle 010 \rangle_{pc}$) of the stripe domains (Fig. 3). To study the switching of the ferroic state, we perform PFM imaging

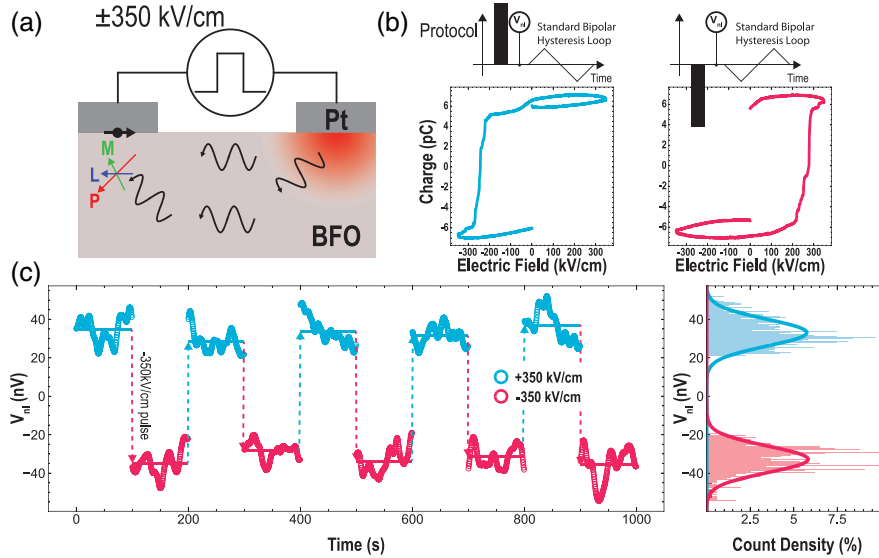


FIG. 2. Bistable states of thermal magnon current. (a) Cross sectional device schematic. As shown by the interfacial spin (black), the detected voltage along the detector (left) wire is dependent on the magnon spin polarization component orthogonal to the length of the Pt wires. (b) Experimental protocol and results of “half” hysteresis loops confirming the stability of the ferroelectric state after electric field poling. (c) Measured lock-in second harmonic voltage, $V_{nl}(2\omega)$, measuring magnon current, as a function of time. 100 sec of data are collected after each electric-field pulse. Data reflect relative changes upon poling, i.e., a small (~ 10 s of nV) dc offset is subtracted from both positively and negatively poled signals. Histogram combining results from 10 trials confirms two distinct states of magnon current. Fits are to normal distributions. An $800 \mu\text{A}$ charge current was used to generate the thermal gradient for SSE.

after application of ± 350 kV/cm across the channel. We observe reversal of the in-plane contrast [Fig. 3(b)], indicating in-plane reversal of the ferroelectric polarization. Importantly, while the in-plane component of the polarization reverses, the underlying ferroelastic domain structure is preserved, i.e., switching occurs within each ferroelastic (stripe) domain. The persistence of the ferroelastic domains very likely contributes to the reversibility

of the magnonic signal observed upon bipolar electric field pulsing [Fig. 2(c)]. The IP PFM results, in combination with out-of-plane (OOP) PFM imaging after switching (Supplemental Material [48], Fig. S2), which does not show reversal, allow us to conclude that polarization switching proceeds via a 71° IP switch, consistent with previous research [36]. We show, schematically [Fig. 3(c)], the resulting reorientation of the polarization, Néel vector,

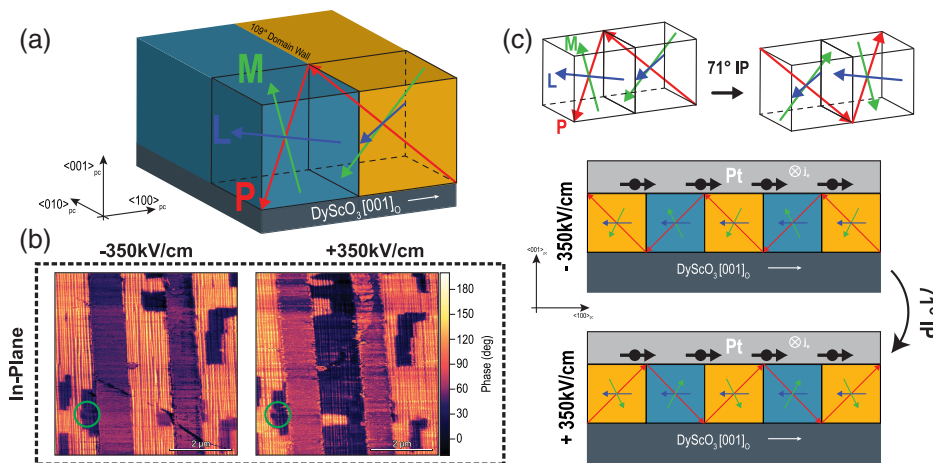


FIG. 3. Switching mechanism. (a) Schematic of twin 109° domains showing ferroelectric polarization vector, \mathbf{P} (red), Néel vector \mathbf{L} (blue), and canted magnetization vector \mathbf{M} (green). (b) In-plane phase PFM images after $+350$ and -350 kV/cm applied across the channel. The change in contrast indicates reversal of the net in-plane polarization (and therefore canted magnetization). A (green) circle marks an external reference domain pattern for comparison. (c) Schematic of 71° IP switch showing reversal of the both the net ferroelectric polarization, \mathbf{P} , and net canted moment, \mathbf{M} .

and canted moment after 71° switching. The ISHE detection mechanism is sensitive to the magnon spin polarization, and therefore the magnetic order, directly beneath the detector Pt wire. Furthermore, since the Pt wire spans several domains, the detected voltage is a function of the adjacent *net* magnetic order (i.e., the sum of twin domain contributions). While magnons have been shown to traverse both **M** and **L** [12,15,19], from the schematic [Fig. 3(c)], one can observe that while the net canted moment, **M**, does reverse, the net Néel vector, **L**, does not reverse following 71° switching. This indicates that our data are sensitive to spin wave excitations carried along (spin polarization antiparallel to) the net canted moment, **M**.

While we have so far discussed thermal magnons, it is important to address another excitation mechanism, namely, the spin accumulation mechanism (SAM) [5,12,19,50] from the spin Hall effect (SHE) in the injector wire. This effect is dependent on the charge current in the injector wire (as opposed to j^2 in SSE) and therefore appears in the first harmonic nonlocal voltage. Electric-field switching of BFO results in no change in the first harmonic signal (Supplemental Material [48], Fig. S3). It has been shown both experimentally [28] and theoretically [56,57] that (anti-)ferromagnetic domain walls act as scattering sites for incident magnons. To observe a first harmonic signal, magnons excited via SAM at the injector must traverse the channel without (or with minimal) scattering. Our PFM data reveal many domain walls between the injector and detector, which scatter all SAM excited magnons, and result in no observed first harmonic signal. Thermal magnons however, can be “reexcited” after a domain wall since the thermal gradient, governed by phonon diffusion, for example, persists. As described in detail in Supplemental Material [48], Secs. 1,2, similar physics can explain the lack of first harmonic signal in multidomain NiO [14], and is corroborated by reports on YIG which study the effects of nonlocal thermal gradients [31] and heat-transparent or spin-opaque interfaces [58].

Having established the mechanism behind magnetization reversal and the observed magnon current, we now demonstrate its hysteretic nature. We perform a quasi-static measurement [Fig. 4(a)], varying the magnitude of the electric field pulse across the channel from negative to positive and back again, while measuring (over 100 sec) the nonlocal signal after each applied electric field pulse. We observe a hysteretic response in the magnon current [Fig. 4(b)] which closely matches the ferroelectric hysteresis loop of the same device. To confirm that the observed data do not stem from capacitive charging or other extrinsic circuit effects [59], we perform the identical measurement on YIG [Fig. 4(b)]. As expected, we observe no ferroelectric hysteresis, and importantly no hysteretic magnon current. Next, to confirm that the signal does not come from the remanent state of the ferroelectric polarization alone, we use a nonmagnetic, in-plane ferroelectric $\text{Pb}_{0.7}\text{Sr}_{0.3}\text{TiO}_3$ (PSTO) (Supplemental

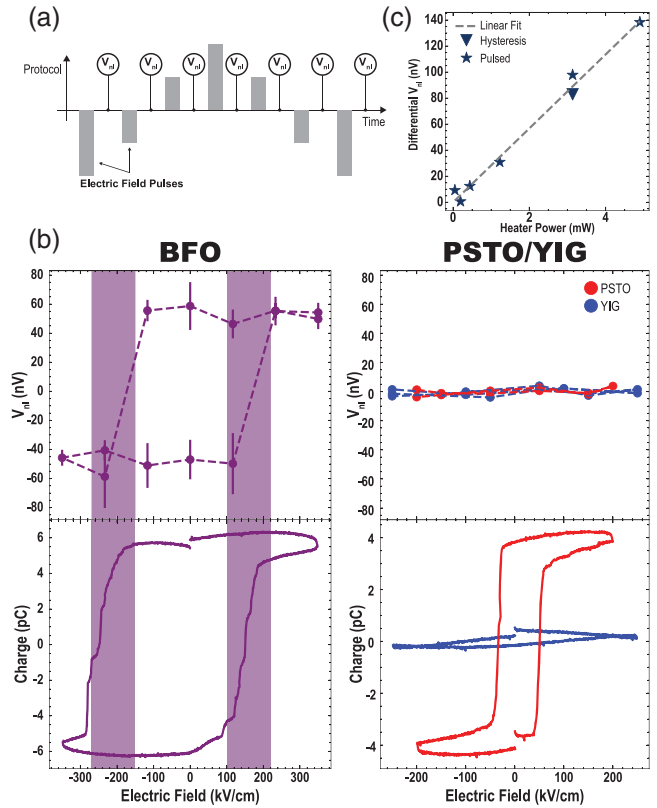


FIG. 4. Hysteretic response. (a) Hysteretic magnon current measurement protocol. (b) Observation of hysteresis in nonlocal second harmonic signal in BFO showing excellent agreement with the associated ferroelectric hysteresis loop. Identical measurements on PSTO and YIG are also shown. (c) Magnitude of differential nonlocal voltage as a function of injector (heater) current, as measured through several different means.

Material [48], Methods) sample with a similar value of switchable charge and again perform the identical experiment [Fig. 4(b)]. Here, we observe a strong ferroelectric hysteresis response, as expected, but do not observe any hysteresis in the nonlocal voltage. The YIG and PSTO control samples together, therefore, allow us to conclude that the BFO signal is magnetic in nature. Finally, as the SSE signal scales with the square of the charge current in the injector wire, we expect a linear dependence on injector (heater) power (I^2R) in the differential nonlocal voltage, defined as the difference between measured nonlocal second harmonic voltage when poled with a positive vs negative electric field. We show [Fig. 4(c)] the expected linear dependence as a function of heater power.

In conclusion, we have demonstrated a novel manifestation of intrinsic magnetoelectric coupling in BFO, establishing electric field control of nonvolatile, hysteretic, bistable states of magnon current in the absence of an applied magnetic field. This represents a crucial step towards operational magnon-based devices. On-going work focuses on several pathways for increasing the

magnitude of the nonlocal voltage for practical applications [41]. By varying the domain structure with choice of substrate [49], one can vary the number and type of magnon scattering sites present between the injector and detector. Advanced lithography techniques can also be utilized to minimize the injector-detector distance, with previous research indicating highly favorable scaling laws for reduced channel widths [12,30]. In fact, with improved magnon coherence and/or decreased channel spacing, domain walls can be written using an out-of-plane electric field (rather than in-plane as demonstrated here), thereby enabling a nonvolatile three terminal transistor which operates on magnon scattering at domain walls at the gate. Perhaps most importantly, however, is the inclusion of alternate spin-orbit (SO) metals (replacing Pt). The spin Hall angle sets an intrinsic limit on the detected voltage, while the interface between the SO metal and the BFO can limit spin conductance and introduce variability in the fabrication process. Oxide SO metals, such as SrIrO₃, have recently shown high spin Hall angles [60], and most importantly can be grown epitaxially, *in situ*, via PLD on BFO, likely allowing for improved spin conductance, higher nonlocal voltages, and lower operating current, while maintaining BFO quality. The results shown here offer an initial verification, highlighting an important synergy between multiferroics and magnonic spintronics, and demonstrating a novel pathway toward functional magnonic devices.

E. P. acknowledges support from the Intel/FEINMAN program. L. C. acknowledges financial support from the Ford Foundation and the University of California President's Postdoctoral Fellowship Program. V. N. is supported by UC National Laboratory Fees Research Program In-Residence Graduate Fellowship Grant No. L21GF3660. H. Z. acknowledges support from the Department of Defense, Air Force Office of Scientific Research under Award No. FA9550-18-1-0480. P. B. acknowledges support from the Office of Science, Basic Energy Sciences (BES) at the Department of Energy (DOE) Contract No. DE-AC02-05CH11231. J. A. acknowledges support from the U.S. Department of Energy, Office of Science, Basic Energy Sciences, Materials Sciences and Engineering Division under Contract No. DE-AC02-05-CH11231 within the Quantum Materials program (KC2202). X. H. and R. R. acknowledges support from the SRC-ASCENT Center, which is part of the SRC JUMP program.

-
- [1] A. V. Chumak, V. I. Vasyuchka, A. A. Serga, and B. Hillebrands, Magnon spintronics, *Nat. Phys.* **11**, 453 (2015).
 [2] A. Barman *et al.*, The 2021 magnonics roadmap, *J. Phys. Condens. Matter* **33**, 413001 (2021).

- [3] S. M. Rezende, *Fundamentals of Magnonics* (Springer, 2020).
 [4] *Magnonics: From Fundamentals to Applications*, edited by S. O. Demokritov and A. N. Slavin (Springer, New York, 2013).
 [5] R. Lebrun, A. Ross, S. A. Bender, A. Qaiumzadeh, L. Baldrati, J. Cramer, A. Brataas, R. A. Duine, and M. Kläui, Tunable long-distance spin transport in a crystalline antiferromagnetic iron oxide, *Nature (London)* **561**, 222 (2018).
 [6] A. Mahmoud, F. Ciubotaru, F. Vanderveken, A. V. Chumak, S. Hamdioui, C. Adelman, and S. Cotofana, Introduction to spin wave computing, *J. Appl. Phys.* **128**, 161101 (2020).
 [7] A. Khitun, M. Bao, and K. L. Wang, Magnonic logic circuits, *J. Phys. D* **43**, 264005 (2010).
 [8] G. Csaba, Á. Papp, and W. Porod, Perspectives of using spin waves for computing and signal processing, *Phys. Lett. A* **381**, 1471 (2017).
 [9] A. V. Chumak, A. A. Serga, and B. Hillebrands, Magnon transistor for all-magnon data processing, *Nat. Commun.* **5**, 4700 (2014).
 [10] J. Lan, W. Yu, R. Wu, and J. Xiao, Spin-Wave Diode, *Phys. Rev. X* **5**, 041049 (2015).
 [11] R. Cheng, M. W. Daniels, J. G. Zhu, and D. Xiao, Antiferromagnetic spin wave field-effect transistor, *Sci. Rep.* **6**, 2 (2016).
 [12] L. J. Cornelissen, J. Liu, R. A. Duine, J. B. Youssef, and B. J. van Wees, Long-distance transport of magnon spin information in a magnetic insulator at room temperature, *Nat. Phys.* **11**, 1022 (2015).
 [13] L. J. Cornelissen, K. J. H. Peters, G. E. W. Bauer, R. A. Duine, and B. J. van Wees, Magnon spin transport driven by the magnon chemical potential in a magnetic insulator, *Phys. Rev. B* **94**, 014412 (2016).
 [14] G. R. Hoogeboom and B. J. van Wees, Nonlocal spin Seebeck effect in the bulk easy-plane antiferromagnet NiO, *Phys. Rev. B* **102**, 214415 (2020).
 [15] R. Lebrun, A. Ross, S. A. Bender, A. Qaiumzadeh, L. Baldrati, J. Cramer, A. Brataas, R. A. Duine, and M. Kläui, Electrically tunable long-distance transport in crystalline antiferromagnetic iron oxide, *Nature (London)* **561**, 222 (2018).
 [16] L. Baldrati *et al.*, Mechanism of Néel Order Switching in Antiferromagnetic Thin Films Revealed by Magnetotransport and Direct Imaging, *Phys. Rev. Lett.* **123**, 177201 (2019).
 [17] A. Ross *et al.*, Propagation length of antiferromagnetic magnons governed by domain configurations, *Nano Lett.* **20**, 306 (2020).
 [18] W. Yuan *et al.*, Experimental signatures of spin superfluid ground state in canted antiferromagnet Cr₂O₃ via nonlocal spin transport, *Sci. Adv.* **4**, eaat1098 (2018).
 [19] J. Han, P. Zhang, Z. Bi, Y. Fan, T. S. Safi, J. Xiang, J. Finley, L. Fu, R. Cheng, and L. Liu, Birefringence-like spin transport via linearly polarized antiferromagnetic magnons, *Nat. Nanotechnol.* **15**, 563 (2020).
 [20] K. Abraha and D. R. Tilley, Theory of far infrared properties of magnetic surfaces, films and superlattices, *Surf. Sci. Rep.* **24**, 129 (1996).

- [21] G. T. Rado and J. R. Weertman, Spin-wave resonance in a ferromagnetic metal, *J. Phys. Chem. Solids* **11**, 315 (1959).
- [22] K. Uchida, S. Takahashi, K. Harii, J. Ieda, W. Koshibae, K. Ando, S. Maekawa, and E. Saitoh, Observation of the spin Seebeck effect, *Nature (London)* **455**, 778 (2008).
- [23] M. W. Daniels, W. Guo, G. M. Stocks, D. Xiao, and J. Xiao, Spin-transfer torque induced spin waves in anti-ferromagnetic insulators, *New J. Phys.* **17**, 103039 (2015).
- [24] C. Liu *et al.*, Electric field control of magnon spin currents in an antiferromagnetic insulator, *Sci. Adv.* **7**, eabg1669 (2021).
- [25] B. L. Giles, Z. Yang, J. S. Jamison, and R. C. Myers, Long-range pure magnon spin diffusion observed in a nonlocal spin-Seebeck geometry, *Phys. Rev. B* **92**, 224415 (2015).
- [26] S. T. B. Goennenwein, R. Schlitz, M. Pernpeintner, K. Ganzhorn, M. Althammer, R. Gross, and H. Huebl, Non-local magnetoresistance in YIG/Pt nanostructures, *Appl. Phys. Lett.* **107**, 172405 (2015).
- [27] L. J. Cornelissen, J. Shan, and B. J. van Wees, Temperature dependence of the magnon spin diffusion length and magnon spin conductivity in the magnetic insulator yttrium iron garnet, *Phys. Rev. B* **94**, 180402 (2016).
- [28] A. Ross *et al.*, Propagation length of antiferromagnetic magnons governed by domain configurations, *Nano Lett.* **20**, 306 (2020).
- [29] W. Xing, L. Qiu, X. Wang, Y. Yao, Y. Ma, R. Cai, S. Jia, X. C. Xie, and W. Han, Magnon Transport in Quasi-Two-Dimensional van der Waals Antiferromagnets, *Phys. Rev. X* **9**, 011026 (2019).
- [30] C. O. Avci, E. Rosenberg, M. Huang, J. Bauer, C. A. Ross, and G. S. D. Beach, Nonlocal Detection of Out-of-Plane Magnetization in a Magnetic Insulator by Thermal Spin Drag, *Phys. Rev. Lett.* **124**, 027701 (2020).
- [31] J. Shan, L. J. Cornelissen, J. Liu, J. B. Youssef, L. Liang, and B. J. van Wees, Criteria for accurate determination of the magnon relaxation length from the nonlocal spin Seebeck effect, *Phys. Rev. B* **96**, 184427 (2017).
- [32] J. B. Neaton, C. Ederer, U. V. Waghmare, N. A. Spaldin, and K. M. Rabe, First-principles study of spontaneous polarization in multiferroic BiFeO₃, *Phys. Rev. B* **71**, 014113 (2005).
- [33] J. Wang *et al.*, Epitaxial BiFeO₃ multiferroic thin film heterostructures, *Science* **299**, 1719 (2003).
- [34] C. Ederer and N. A. Spaldin, Weak ferromagnetism and magnetoelectric coupling in bismuth ferrite, *Phys. Rev. B* **71**, 060401 (2005).
- [35] T. Zhao *et al.*, Electrical control of antiferromagnetic domains in multiferroic BiFeO₃ films at room temperature, *Nat. Mater.* **5**, 823 (2006).
- [36] J. T. Heron *et al.*, Deterministic switching of ferromagnetism at room temperature using an electric field, *Nature (London)* **516**, 370 (2014).
- [37] B. Prasad *et al.*, Ultralow voltage manipulation of ferromagnetism, *Adv. Mater.* **32**, 2001943 (2020).
- [38] A. Haykal *et al.*, Antiferromagnetic textures in BiFeO₃ controlled by strain and electric field, *Nat. Commun.* **11**, 1704 (2020).
- [39] Y.-L. Huang *et al.*, Manipulating magnetoelectric energy landscape in multiferroics, *Nat. Commun.* **11**, 2836 (2020).
- [40] S. Manipatruni, D. E. Nikonov, and I. A. Young, Beyond CMOS computing with spin and polarization, *Nat. Phys.* **14**, 338 (2018).
- [41] S. Manipatruni, D. E. Nikonov, C.-C. Lin, T. A. Gosavi, H. Liu, B. Prasad, Y.-L. Huang, E. Bonturim, R. Ramesh, and I. A. Young, Scalable energy-efficient magnetoelectric spin-orbit logic, *Nature (London)* **565**, 35 (2019).
- [42] E. Parsonnet, Y.-L. Huang, T. Gosavi, A. Qualls, D. Nikonov, C.-C. Lin, I. Young, J. Bokor, L. W. Martin, and R. Ramesh, Toward Intrinsic Ferroelectric Switching in Multiferroic BiFeO₃, *Phys. Rev. Lett.* **125**, 067601 (2020).
- [43] P. Rovillain, R. de Sousa, Y. Gallais, A. Sacuto, M. A. Méasson, D. Colson, A. Forget, M. Bibes, A. Barthélémy, and M. Cazayous, Electric-field control of spin waves at room temperature in multiferroic BiFeO₃, *Nat. Mater.* **9**, 975 (2010).
- [44] A. Kumar, J. F. Scott, and R. S. Katiyar, Electric control of magnon frequencies and magnetic moment of bismuth ferrite thin films at room temperature, *Appl. Phys. Lett.* **99**, 062504 (2011).
- [45] R. de Sousa and J. E. Moore, Electrical control of magnon propagation in multiferroic BiFeO₃ films, *Appl. Phys. Lett.* **92**, 022514 (2008).
- [46] J. E. Hirsch, Spin Hall Effect, *Phys. Rev. Lett.* **83**, 1834 (1999).
- [47] A. V. Chumak, A. A. Serga, M. B. Jungfleisch, R. Neb, D. A. Bozhko, V. S. Tiberkevich, and B. Hillebrands, Direct detection of magnon spin transport by the inverse Spin Hall effect, *Appl. Phys. Lett.* **100**, 082405 (2012).
- [48] See Supplemental Material at <http://link.aps.org/supplemental/10.1103/PhysRevLett.129.087601> for extended data and discussion.
- [49] L. W. Martin, Engineering multiferroic materials and new functionalities in materials, Doctoral Thesis, University of California, Berkeley, Berkeley, CA, 2008.
- [50] S. S.-L. Zhang and S. Zhang, Spin convertance at magnetic interfaces, *Phys. Rev. B* **86**, 214424 (2012).
- [51] E. Parsonnet, Ekpy (2022), <https://github.com/eparsonnet93/ekpmeasure>.
- [52] S. Huang *et al.*, Multiferroic behavior from synergetic response of multiple ordering parameters in BiFeO₃ single crystal under high magnetic field up to 50 Tesla, *J. Appl. Phys.* **127**, 044101 (2020).
- [53] T. Zhao *et al.*, Electrical control of antiferromagnetic domains in multiferroic BiFeO₃ films at room temperature, *Nat. Mater.* **5**, 823 (2006).
- [54] Y.-C. Liao, D. E. Nikonov, S. Dutta, S.-C. Chang, C.-S. Hsu, I. A. Young, and A. Naeemi, Understanding the switching mechanisms of the antiferromagnet/ferromagnet heterojunction, *Nano Lett.* **20**, 7919 (2020).
- [55] J. T. Heron, M. Trassin, K. Ashraf, M. Gajek, Q. He, S. Y. Yang, D. E. Nikonov, Y.-H. Chu, S. Salahuddin, and R. Ramesh, Electric-Field-Induced Magnetization Reversal in a Ferromagnet-Multiferroic Heterostructure, *Phys. Rev. Lett.* **107**, 217202 (2011).
- [56] J. Lan, W. Yu, and J. Xiao, Antiferromagnetic domain wall as spin wave polarizer and retarder, *Nat. Commun.* **8**, 1 (2017).

- [57] W. Yu, J. Lan, and J. Xiao, Polarization-selective spin wave driven domain-wall motion in antiferromagnets, *Phys. Rev. B* **98**, 144422 (2018).
- [58] J. Shan, L. J. Cornelissen, N. Vlietstra, J. B. Youssef, T. Kuschel, R. A. Duine, and B. J. van Wees, Influence of yttrium iron garnet thickness and heater opacity on the nonlocal transport of electrically and thermally excited magnons, *Phys. Rev. B* **94**, 174437 (2016).
- [59] F. Volmer, T. Bisswanger, A. Schmidt, C. Stampfer, and B. Beschoten, Charge-induced artifacts in non-local spin transport measurements: How to prevent spurious voltage signals, [arXiv:2112.02047](https://arxiv.org/abs/2112.02047).
- [60] X. Huang *et al.*, Novel spin-orbit torque generation at room temperature in an all-oxide epitaxial $\text{La}_{0.7}\text{Sr}_{0.3}\text{MnO}_3/\text{SrIrO}_3$ system, *Adv. Mater.* **33**, 2008269 (2021).